Electronic Supplementary Material (ESI) for Dalton Transactions.

Electronic Supplementary Information (ESI):

Reversible Binding of Dinitrogen on a Thiolate-Bridged Cobalt-Ruthenium Complex Supported by a Flexible Bidentate Phosphine Ligand

Wenjing Dong,[a] Dawei Yang,*[a] Tao Mei,[a] Baomin Wang[a] and Jingping Qu[a]

[a]*State Key Laboratory of Fine Chemicals, Dalian University of Technology, Dalian 116024, P. R. China*

E-mail: yangdw@dlut.edu.cn

Table of Contents

I. General Materials and Methods

General Consideration. All manipulations were performed under an argon atmosphere by standard Schlenk techniques unless otherwise specified. All solvents were dried and distilled over an appropriate drying agent under argon. [Cp*Co(η^3-tpdt)] (Cp* = η^5-C_5Me_5, tpdt = $S(CH_2CH_2S^-)_2$),[1] and [$RuCl_2(PPh_3)_3$][2] were prepared according to literature procedures. 1,2-Bis(diphenylphosphino)ethane (dppe, Heowns), $NaBPh_4$ (Aldrich), N_2 and $^{15}N_2$ (Dalian Junfeng Gas chemical Co., LTD) are commercially available and used as received without further purification.

Spectroscopic Measurements. NMR spectra were recorded on a Brüker 400 Ultra Shield spectrometer (400 MHz for ^1H; 162 MHz for $^{31}P\{^1H\}$; 40.6 MHz for ^{15}N). The chemical shifts (δ) are given in parts per million relative to CD_2Cl_2 (5.32 ppm for ^1H). ^{15}N chemical shifts are referenced to external nitromethane (δ = 380.74 ppm relative to liquid ammonia at 0 ppm). Infrared spectra were recorded on a NEXVS FT-IR spectrometer. ESI-HRMS analyses were recorded on a UPLC/Q-Tof micro-spectrometer. Elemental analyses were performed on a Vario EL analyzer. GC analyses were performed using an Agilent 6890N gas chromatography system equipped with an Agilent DB-5MS 30 m × 0.25 mm column and FID detector and a Techcomp GC7900 gas chromatography instrument with argon as the carrier gas and a thermal conductivity detector. Absorption spectra were recorded with an Agilent UV-8453 spectrophotometer.

X-ray Crystallography Procedures. Single-crystal X-ray diffraction studies were carried out on a Brüker SMART APEX CCD diffractometer with graphite-monochromated Mo Kα radiation (λ = 0.71073 Å). Empirical absorption corrections were performed using the SADABS program.[3] All structures were solved with the Superflip structure solution program using Charge Flipping and refined with the XL refinement package using least Squares minimization that implanted in Olex2.[3-6] All of the non-hydrogen atoms were refined anisotropically. All of the hydrogen atoms were generated and refined in ideal positions.

II. Experimental Procedures and Analytical Data

Synthesis of [Cp*Co(μ-1κ^3*SSS′*:2κ^2*SS*-tpdt)$RuCl_2(PPh_3)_2$] (1). [$RuCl_2(PPh_3)_3$] (958 mg, 1.00 mmol) was added to a solution of [Cp*Co(η^3-tpdt)] (345 mg, 1.00 mmol) in THF (50 mL) at room temperature. The solution color rapidly changed from purple to brown. The reaction mixture was stirred at room temperature for 4 h. After removal of the solvent, the solids were washed with Et_2O (30 mL × 3), and dried under vacuum to afford a brown powder **1** (573 mg, 0.55 mmol, 55%). Single-crystals suitable for X-ray diffraction analysis were grown by slow diffusion of *n*-hexane into a CH_2Cl_2 solution of **1** at room temperature. ^{1}H NMR (400 MHz, CD_2Cl_2, ppm): δ 0.92 (m, 2H, tpdt-*H*), 2.06–3.65 (m, 6H, tpdt-*H*), 7.11–7.55 (m, 30H, Ph-*H*), 1.45 (s, 15H, Cp*-CH_3). ^{31}P{^{1}H} NMR (162 MHz, CD_2Cl_2, ppm): δ 40.31 (s). IR (KBr, cm^{-1}): 3051, 2962, 2903, 1483, 1433, 1260, 1090, 1026, 807, 742, 692. Anal. Calcd for $C_{50}H_{53}Cl_2CoP_2RuS_3$: C, 57.58; H, 5.12. Found: C, 57.53; H, 5.24.

Synthesis of [Cp*Co(μ-1κ^3*SSS′*:2κ^2*SS*-tpdt)RuCl(PPh_3)$_2$][BPh_4] (2). Complex **1** (104 mg, 0.10 mmol) and $NaBPh_4$ (34 mg, 0.10 mmol) were dissolved in CH_2Cl_2 (8 mL) and stirred at room temperature for 10 h. The resulting brown-red solution was filtered and dried in vacuum to provide a dark-brown powder **2** (80 mg, 0.06 mmol, 60%). Crystals suitable for X-ray diffraction analysis were obtained from a THF solution layered with Et_2O at room temperature. ^{1}H NMR (400 MHz, CD_2Cl_2, ppm, **2**·Et_2O): δ 1.82 (m, 4H, tpdt-*H*), 3.68 (m, 4H, tpdt-*H*), 1.15 (m, 6H, Et_2O-CH_3), 3.44 (m, 4H, Et_2O-CH_2), 6.86–7.30 (m, 50H, Ph-*H*), 1.36 (s, 15H, Cp*-CH_3). ^{31}P{^{1}H} NMR (162 MHz, CD_2Cl_2, ppm): δ 37.15 (s), 74.45 (s). IR (KBr, cm^{-1}): 3055, 2916, 2854, 1579, 1481, 1433, 1261, 1088, 1032, 702. HRMS (ESI, *m/z*) calcd for $C_{50}H_{53}ClCoP_2RuS_3$ [**2**−BPh_4]$^+$, 1007.0862, found 1007.0864. Anal. Calcd for $C_{74}H_{73}BClCoP_2RuS_3$: C, 66.99; H, 5.55. Found: C, 66.61; H, 5.92.

Synthesis of [Cp*Co(μ-1κ^3*SSS′*:2κ^2*SS*-tpdt)RuCl_2(dppe)] (3). To a solution of **1** (104 mg, 0.10 mmol) in CH_2Cl_2 (8 mL) was added 1,2-bis(diphenylphosphino)ethane (dppe, 40 mg, 0.10 mmol) at room temperature. The solution color rapidly changed from brown to yellow. The reaction mixture was stirred at room temperature for 4 h. After all volatiles were removed under vacuum, the residue was washed with Et_2O (10 mL × 3) and then dried under vacuum. The product **3** (58 mg, 0.063 mmol, 63%) was obtained as a yellow-green powder. Single-crystals suitable for X-ray diffraction analysis were grown by slow diffusion of *n*-hexane into a CH_2Cl_2 solution of **3** at room temperature. ^{1}H NMR (400 MHz, CD_2Cl_2, ppm): δ 1.74–2.40 (m, 4H, $PPh_2(CH_2)_2PPh_2$), 2.58–3.80 (m, 8H, tpdt-*H*), 7.19–8.01 (m, 20H, Ph-*H*), 1.62 (s, 15H, Cp*-CH_3). ^{31}P{^{1}H} NMR (162 MHz, CD_2Cl_2, ppm): δ 59.48 (s). IR (KBr, cm^{-1}): 3053, 2908, 1485, 1433, 1373, 1097, 1026, 746, 696. Anal. Calcd for $C_{40}H_{47}Cl_2CoP_2RuS_3$: C, 52.40; H, 5.17. Found: C, 52.33; H, 5.47.

Synthesis of [Cp*Co(μ-1κ^3*SSS′*:2κ^2*SS*-tpdt)RuCl(N_2)(dppe)][BPh_4] (4). Under a dinitrogen atmosphere, $NaBPh_4$ (34 mg, 0.10 mmol) was added to a solution of **3** (92 mg, 0.10 mmol) in CH_2Cl_2 (8 mL) at room temperature. The mixture was stirred for 10 h and the color of the reaction solution gradually changed from yellow to brown-red. The resulting solution was filtered and dried in vacuum to provide a dark-brown powder **4** (87 mg, 0.71 mmol, 71%). Single-crystals suitable for X-ray diffraction analysis were grown by slow diffusion of *n*-hexane into a CH_2Cl_2 solution of **4** at room temperature. ^1H NMR (400 MHz, CD_2Cl_2, ppm): δ 1.68–2.44 (m, 4H, $PPh_2(CH_2)_2PPh_2$), 2.62–3.46 (m, 8H, tpdt-*H*), 6.87–7.87 (m, 40H, Ph-*H*), 1.60 (s, 15H, Cp*-CH_3). $^{31}P\{^1H\}$ NMR (162 MHz, CD_2Cl_2, ppm): δ 51.85 (s). IR (KBr, cm^{-1}): 3053, 2981, 2908, 2131($\nu_{N\equiv N}$), 1579, 1483, 1435, 1375, 1120, 825, 702. HRMS (ESI, *m/z*) calcd for $C_{40}H_{47}ClCoN_2P_2RuS_3$ [**4**−BPh_4]$^+$, 909.0452, found 909.0455. There is no satisfactory data of elemental analysis obtained even though several attempts have been made due to its thermal instability.

A sample of ^{15}N-**4** was synthesized using an analogous synthetic procedure starting from $^{15}N_2$ in 64% yield. The ^1H NMR spectrum of ^{15}N-**4** is similar to that of the unlabeled complex **4**. ^{15}N NMR (40.569 MHz, CD_2Cl_2, ppm): δ 297.27 (d, J = 4.0 Hz, Ru−N_α≡N), 310.22 (s, free N_2), 339.22 (d, J = 4.0 Hz, Ru−N≡N_β). IR (KBr, cm^{-1}): 3053, 2981, 2912, 2060($\nu_{15N\equiv 15N}$), 1579, 1481, 1435, 1265, 1097, 814, 704.

Synthesis of [Cp*Co(μ-1κ^3*SSS′*:2κ^2*SS*-tpdt)RuCl(dppe)][BPh_4] (5). Complex **3** (92 mg, 0.10 mmol) and $NaBPh_4$ (34 mg, 0.10 mmol) were dissolved in CH_2Cl_2 (8 mL) and stirred at room temperature for 10 h. The resulting brown-red solution was filtered and dried in vacuum to provide a dark-brown powder **5** (67 mg, 0.56 mmol, 56%). Single-crystals suitable for X-ray diffraction analysis were grown by slow diffusion of *n*-hexane into a CH_2Cl_2 solution of **5** at room temperature. ^1H NMR (400 MHz, CD_2Cl_2, ppm): δ 1.83 (m, 4H, $PPh_2(CH_2)_2PPh_2$), 2.23–3.62 (m, 8H, tpdt-*H*), 6.86–7.47 (m, 40H, Ph-*H*), 1.31 (s, 15H, Cp*-CH_3). $^{31}P\{^1H\}$ NMR (162 MHz, CD_2Cl_2, ppm): δ 65.67 (s), 92.77 (s). IR (KBr, cm^{-1}): 3055, 2981, 2914, 1579, 1481, 1433, 1377, 1095, 816, 704, 613. HRMS (ESI, *m/z*) calcd for $C_{40}H_{47}ClCoP_2RuS_3$ [**5**−BPh_4]$^+$, 881.0385, found 881.0370. Anal. Calcd for $C_{64}H_{67}BClCoP_2RuS_3$: C, 64.03; H, 5.63. Found: C, 63.80; H, 5.81.

Typical procedure for the catalytic reduction of N_2 to $N(SiMe_3)_3$. In a Schlenk flask equipped with a stir bar, KC_8 (135 mg, 1000 μmol) was suspended in THF (5 mL). Me_3SiCl (127 μL, 1000 μmol) was added to the suspension, followed by a solution of catalyst in THF (50 μL, 20 mM, 1.0 μmol). The reaction mixture was stirred at room temperature for 24 h. After addition of dodecane (10 μL) as an internal standard for gas chromatography (GC) analysis, graphite and KCl were removed by filtration. The resultant clear filtrate was subjected to GC analyses. Yields of $N(SiMe_3)_3$ were determined as the average of at least three trials.

III. References

1. Y. Zhang, D. Yang, Y. Li, X. Zhao, B. Wang and J. Qu, *Catal. Sci. Technol.*, 2019, **9**, 6492−6502.
2. Z. Xu, H. Gong, M. Chen, R. Luo, W. Qian, Q. Peng and Z. Hou, *Catal. Commun.*, 2019, **129**, 105743−105747.
3. G. M. Sheldrick, *SADABS, Program for Area Detector Adsorption Correction, Institute for Inorganic Chemistry*, University of Göttingen: Germany, 1996.
4. L. Palatinus and G. Chapuis, *J. Appl. Crystallogr.*, 2007, **40**, 786−790.
5. O. V. Dolomanov, L. J. Bourhis, R. J. Gildea, J. A. K. Howard and H. Puschmann, *J. Appl. Crystallogr.*, 2009, **42**, 339−341.
6. G. M. Sheldrick, *Acta Crystallogr., Sect. A: Found. Adv.*, 2015, **71**, 3−8.

IV. X-ray Crystallographic Data

Table S1. Crystallographic data for **1**, **2**·Et_2O·THF and **3**.

	1	**2**·Et_2O·THF	**3**·THF
Formula	$C_{50}H_{53}Cl_2CoP_2RuS_3$	$C_{82}H_{91}BClCoO_2P_2RuS_3$	$C_{44}H_{55}Cl_2CoOP_2RuS_3$
Formula weight	1042.94	1472.92	988.90
Crystal dimensions (mm^3)	0.20 × 0.12 × 0.10	0.24 × 0.16 × 0.12	0.40 × 0.21 × 0.18
Crystal system	Monoclinic	Monoclinic	triclinic
Space group	$P2_1/n$	$P2_1/c$	P-1
a (Å)	13.0207(7)	11.460(3)	11.4855(10)
b (Å)	24.9378(13)	30.325(6)	12.5440(11)
c (Å)	14.6486(7)	21.269(4)	15.9637(14)
α (°)	90	90	94.842(2)
β (°)	104.173(1)	94.809(4)	105.592(2)
γ (°)	90	90	93.863(2)
Volume ($Å^3$)	4611.7(4)	7366(3)	2197.7(3)
Z	4	4	2
T (K)	220.0	233.0	295.0
D_{calcd} (g cm^{-3})	1.502	1.328	1.494
μ (mm^{-1})	1.043	0.642	1.092
F (000)	2144	3080	1020
No. of rflns. collected	60775	68494	35296
No. of indep. rflns. / R_{int}	9928 / 0.0401	12976 / 0.1347	10702 / 0.0744
No. of obsd. rflns. [$I_0 > 2\sigma(I_0)$]	8666	8025	6177
Data / restraints / parameters	9928 / 1 / 556	12976 / 64 / 845	10702 / 71 / 492
R_1 / wR_2 [$I_0 > 2\sigma(I_0)$]	0.0327 / 0.0773	0.0749 / 0.1578	0.0581 / 0.1031
R_1 / wR_2 (all data)	0.0409 / 0.0841	0.1394 / 0.1777	0.1323 / 0.1268
GOF (on F^2)	1.120	1.062	1.021
Largest diff. peak and hole (e $Å^{-3}$)	0.52 / −0.60	1.45 / −1.04	0.70 / −0.84
CCDC No.	2161675	2161676	2161677

Table S2. Crystallographic data for **4** ·CH_2Cl_2 and **5** ·CH_2Cl_2.

	4 ·CH_2Cl_2	**5** ·CH_2Cl_2
Formula	$C_{65}H_{69}BCl_3CoN_2P_2RuS_3$	$C_{65}H_{69}BCl_3CoP_2RuS_3$
Formula weight	1313.50	1285.48
Crystal dimensions (mm^3)	0.18 × 0.13 × 0.12	0.22 × 0.17 × 0.15
Crystal system	monoclinic	monoclinic
Space group	$P2_1/c$	$P2_1/n$
a (Å)	12.0693(9)	12.0693(10)
b (Å)	14.2710(10)	27.421(2)
c (Å)	35.980(3)	18.1837(15)
α (°)	90	90
β (°)	93.294(2)	101.051(2)
γ (°)	90	90
Volume ($Å^3$)	6186.9(8)	5906.5(8)
Z	4	4
T (K)	200.0	200.0
D_{calcd} (g cm^{-3})	1.410	1.446
μ (mm^{-1})	0.836	0.873
F (000)	2712	2656
No. of rflns. collected	59823	64814
No. of indep. rflns. / R_{int}	10888 / 0.0857	14408 / 0.0777
No. of obsd. rflns. [$I_0 > 2\sigma(I_0)$]	7782	8880
Data / restraints / parameters	10888 / 1125 / 964	14408 / 1 / 690
R_1 / wR_2 [$I_0 > 2\sigma(I_0)$]	0.0932 / 0.1776	0.0537 / 0.0981
R_1 / wR_2 (all data)	0.1330 / 0.1882	0.1166 / 0.1188
GOF (on F^2)	1.164	1.016
Largest diff. peak and hole (e $Å^{-3}$)	1.01 / −1.08	1.12 / −0.62
CCDC No.	2161678	2161679

Figure S1. ORTEP diagram of **1**. Thermal ellipsoids are shown at 50% probability level. All hydrogen atoms are omitted for clarity.

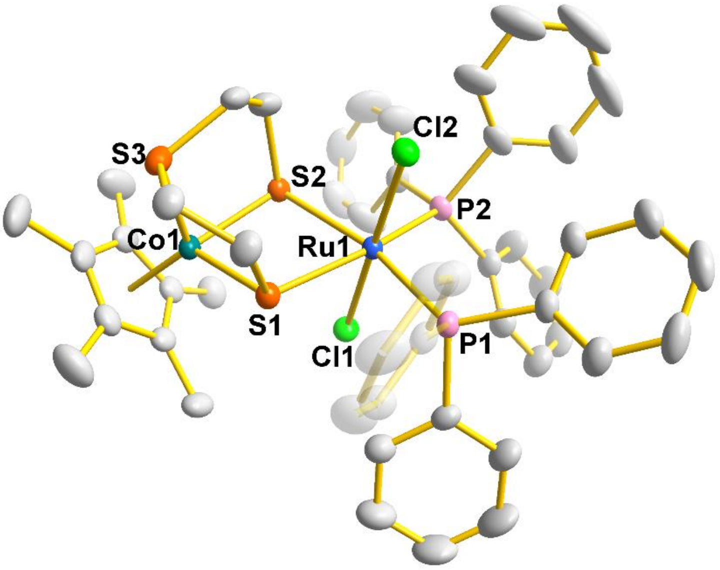

Table S3. Selected bond distances and angles for **1**.

Distances (Å)			
Co1···Ru1	3.5600(2)		
Co1–S1	2.2552(1)	Ru1–S1	2.4647(1)
Ru1–Cl1	2.4025(1)	Ru1–Cl2	2.4166(1)
Ru1–P1	2.3492(1)	Ru1–P2	2.3469(1)
Angles (°)			
Co1–S1–Ru1	97.82(2)	Co1–S2–Ru1	98.33(2)
Torsion angle (°)			
S1–Co1Ru1–S2	164.603(3)		

Figure S2. ORTEP diagram of **2**·Et$_2$O·THF. Thermal ellipsoids are shown at 50% probability level. The non-coordinate Et$_2$O and THF molecule, all hydrogen atoms and the BPh$_4^-$ anion are omitted for clarity.

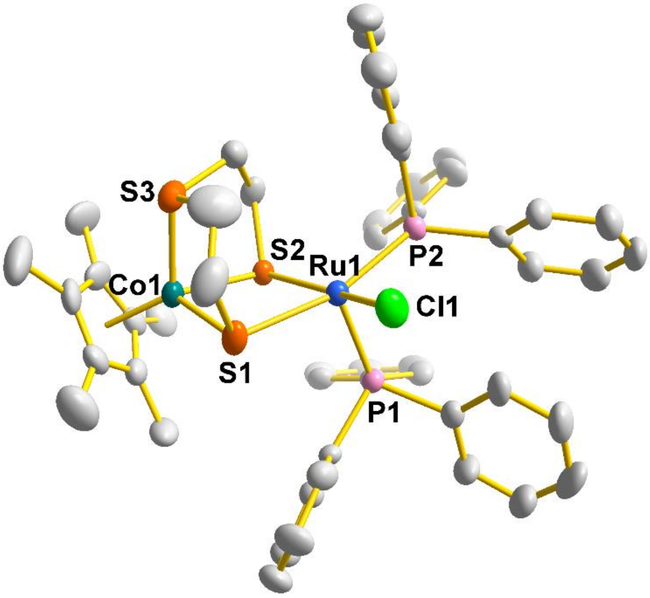

Table S4. Selected bond distances and angles for **2**·Et$_2$O·THF.

Distances (Å)			
Co1···Ru1	3.5045(13)		
Co1–S1	2.2336(18)	Ru1–S1	2.4412(17)
Co1–S3	2.2076(19)	Ru1–Cl1	2.3942(18)
Ru1–P1	2.2283(18)	Ru1–P2	2.3310(18)
Angles (°)			
Co1–S1–Ru1	97.03(6)	Co1–S2–Ru1	99.44(6)
Torsion angle (°)			
S1–Co1Ru1–S2	163.542(95)		

Figure S3. ORTEP diagram of **3**·THF. Thermal ellipsoids are shown at 50% probability level. The non-coordinate THF molecule, all hydrogen atoms are omitted for clarity.

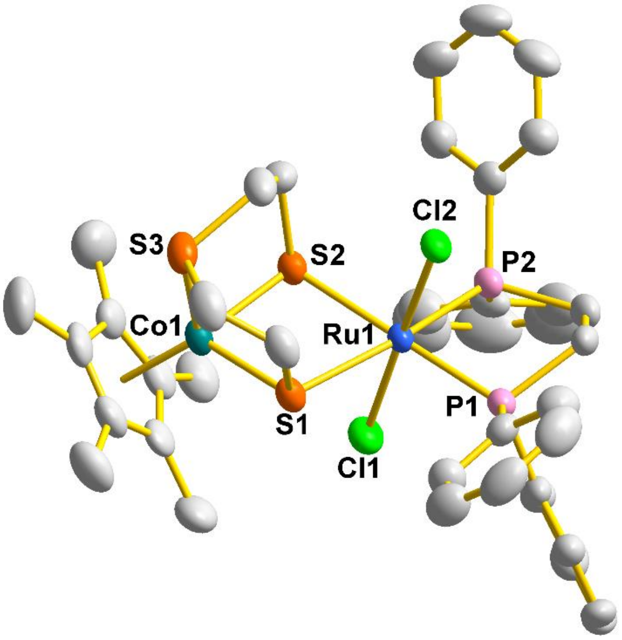

Table S5. Selected bond distances and angles for **3**·THF.

Distances (Å)			
Co1···Ru1	3.5445(8)		
Co1–S1	2.2446(13)	Ru1–S1	2.4421(13)
Ru1–Cl1	2.3946(11)	Ru1–Cl2	2.4431(10)
Ru1–P1	2.2542(12)	Ru1–P2	2.2733(14)
Angles (°)			
Co1–S1–Ru1	98.19(4)	Co1–S2–Ru1	95.47(4)
Torsion angle (°)			
S1–Co1Ru1–S2	165.065(65)		

Figure S4. ORTEP diagram of **4** CH_2Cl_2. Thermal ellipsoids are shown at 50% probability level. All disordered atoms, non-coordinate CH_2Cl_2 molecule, all hydrogen atoms and the BPh_4^- anion are omitted for clarity.

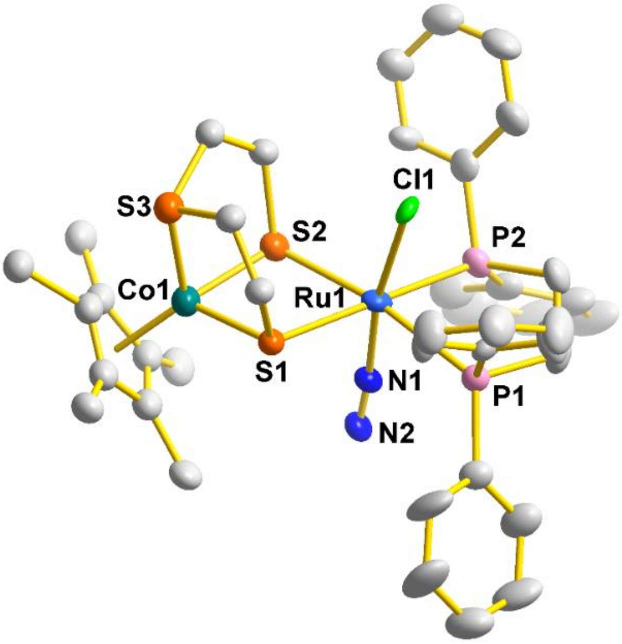

Table S6. Selected bond distances and angles for **4** CH_2Cl_2.

Distances (Å)			
Co1···Ru1	3.547(15)		
Co1–S1	2.173(19)	Ru1–S1	2.441(15)
Ru1–Cl1	2.374(16)	Ru1–N1	1.965(20)
Ru1–P1	2.535(9)	N1–N2	1.022(40)
Angles (°)			
Co1–S1–Ru1	100.3(7)	Ru1–N1–N2	166.4(23)
Torsion angle (°)			
S1–Co1Ru1–S2	167.6(10)		

Figure S5. ORTEP diagram of **5** CH_2Cl_2. Thermal ellipsoids are shown at 50% probability level. The non-coordinate CH_2Cl_2 molecule, all hydrogen atoms and the BPh_4^- anion are omitted for clarity.

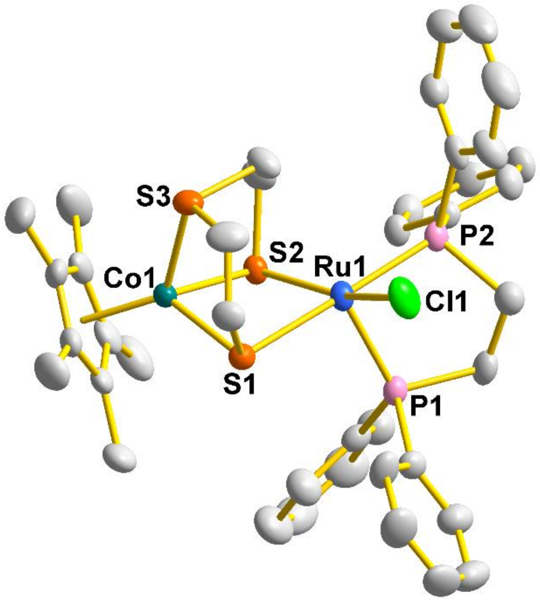

Table S7. Selected bond distances and angles for **5** CH_2Cl_2.

Distances (Å)			
Co1···Ru1	3.3744(2)		
Co1–S1	2.2357(2)	Ru1–S1	2.4306(1)
Co1–S3	2.2199(1)	Ru1–Cl1	2.4001(1)
Ru1–P1	2.2138(1)	Ru1–P2	2.2925(1)
Angles (°)			
Co1–S1–Ru1	92.535(4)	Co1–S2–Ru1	94.937(4)
Torsion angle (°)			
S1–Co1Ru1–S2	152.504(5)		

V. NMR Spectra

Figure S6. The ^{1}H NMR spectrum of **1** in CD_2Cl_2.

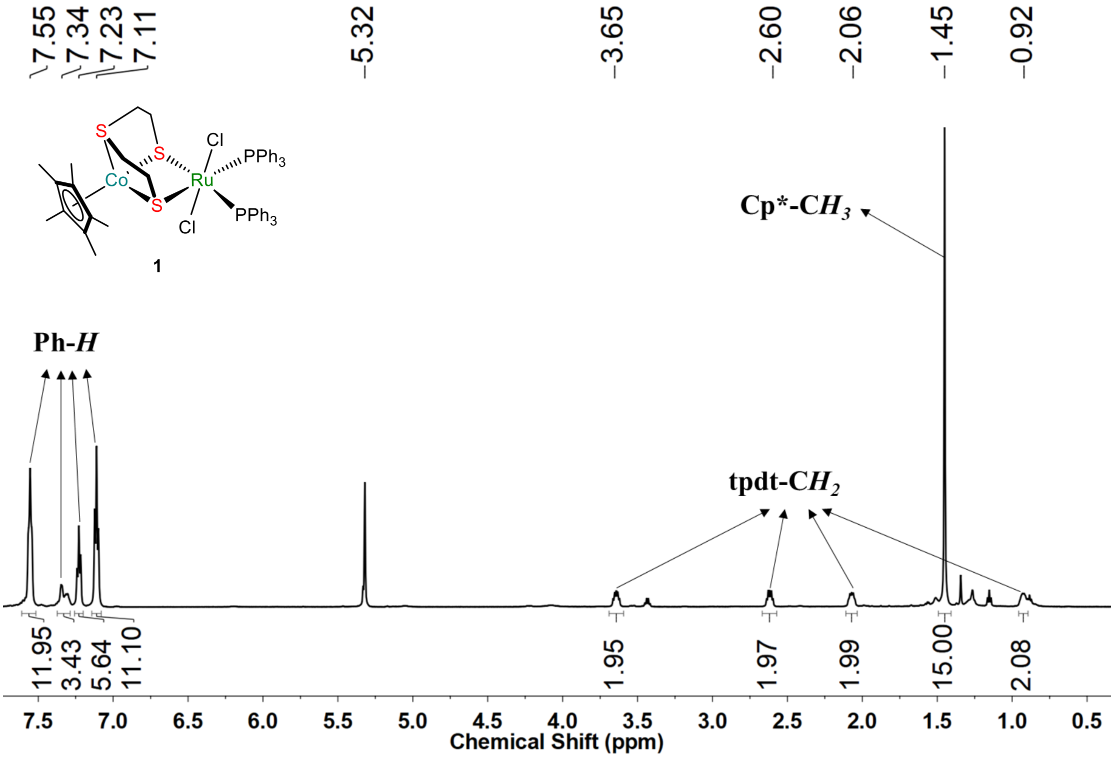

Figure S7. The ^{31}P{^{1}H} NMR spectrum of **1** in CD_2Cl_2.

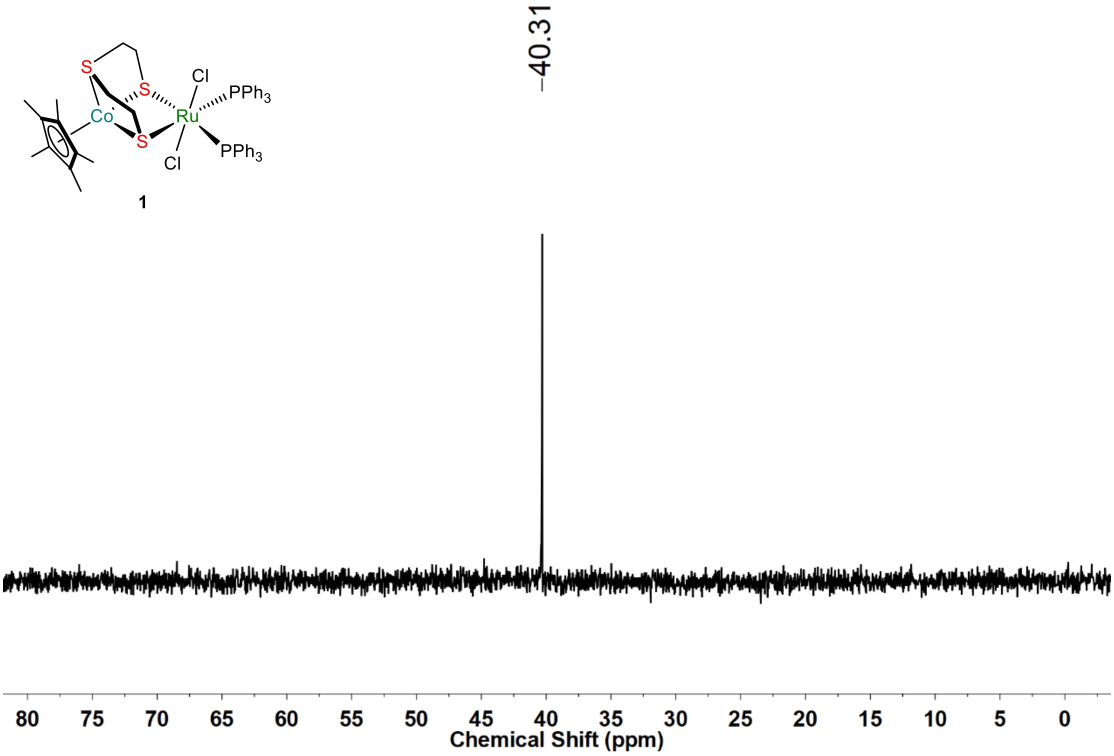

Figure S8. The ^{1}H NMR spectrum of **2** in CD_2Cl_2.

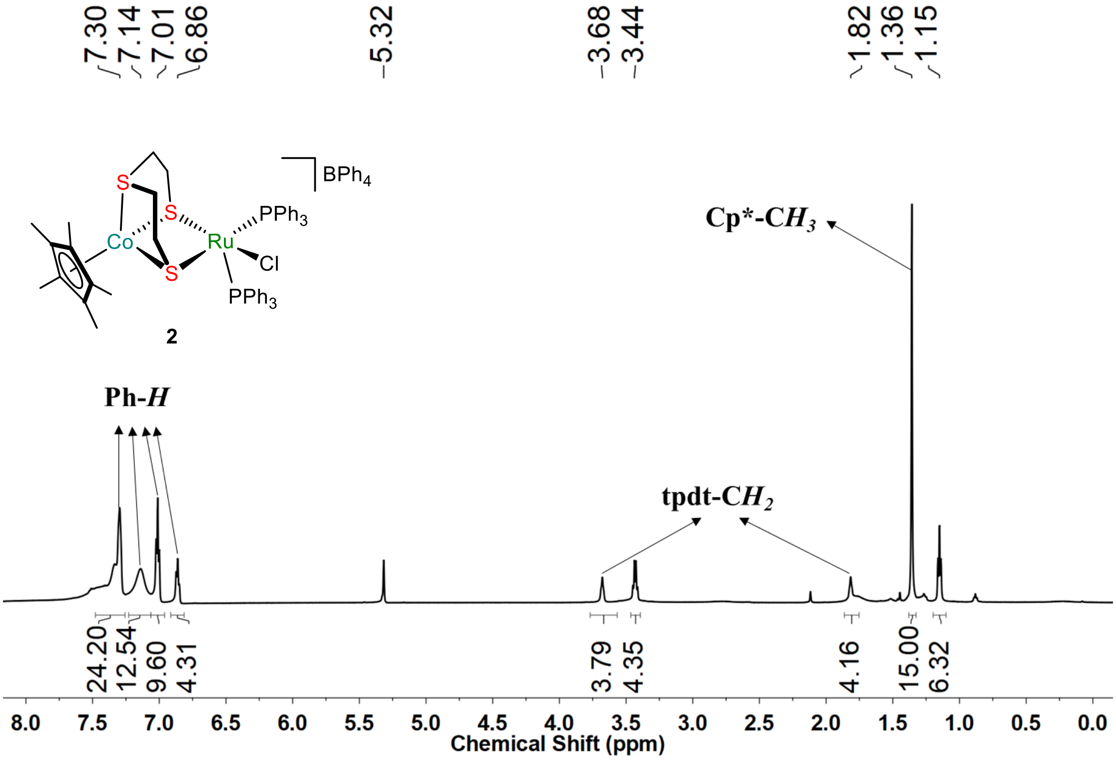

Figure S9. The $^{31}P\{^{1}H\}$ NMR spectrum of **2** in CD_2Cl_2.

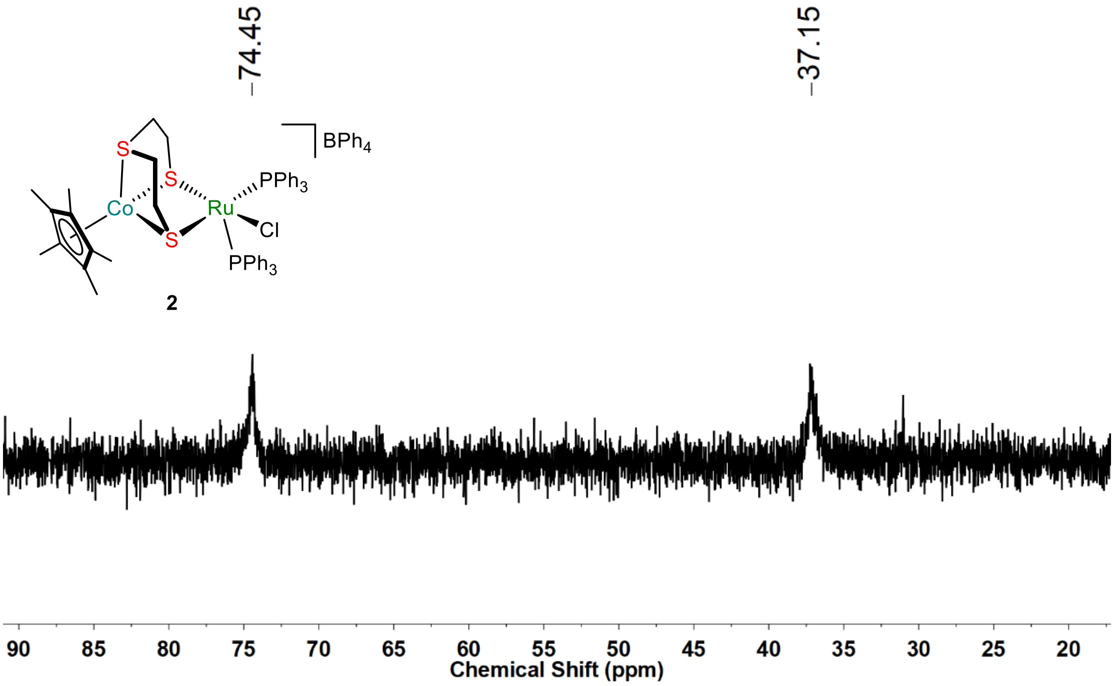

Figure S10. The ^{1}H NMR spectrum of **3** in CD_2Cl_2.

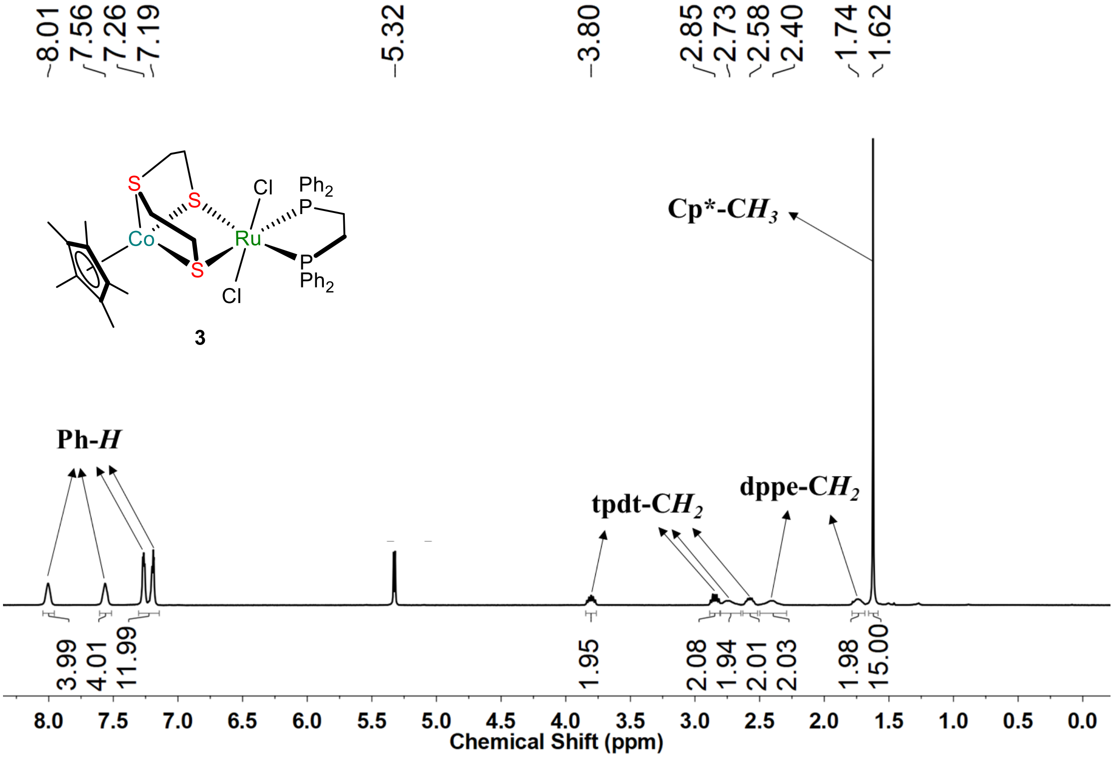

Figure S11. The $^{31}P\{^{1}H\}$ NMR spectrum of **3** in CD_2Cl_2.

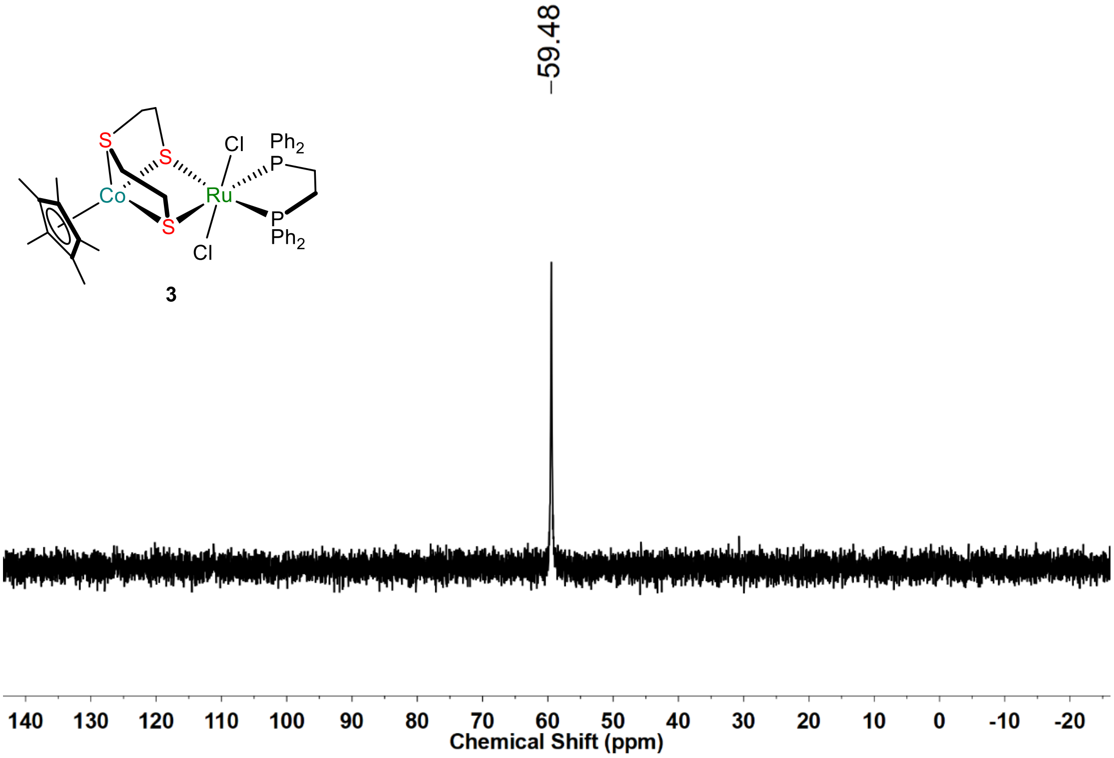

Figure S12. The ^{1}H NMR spectrum of **4** in CD_2Cl_2.

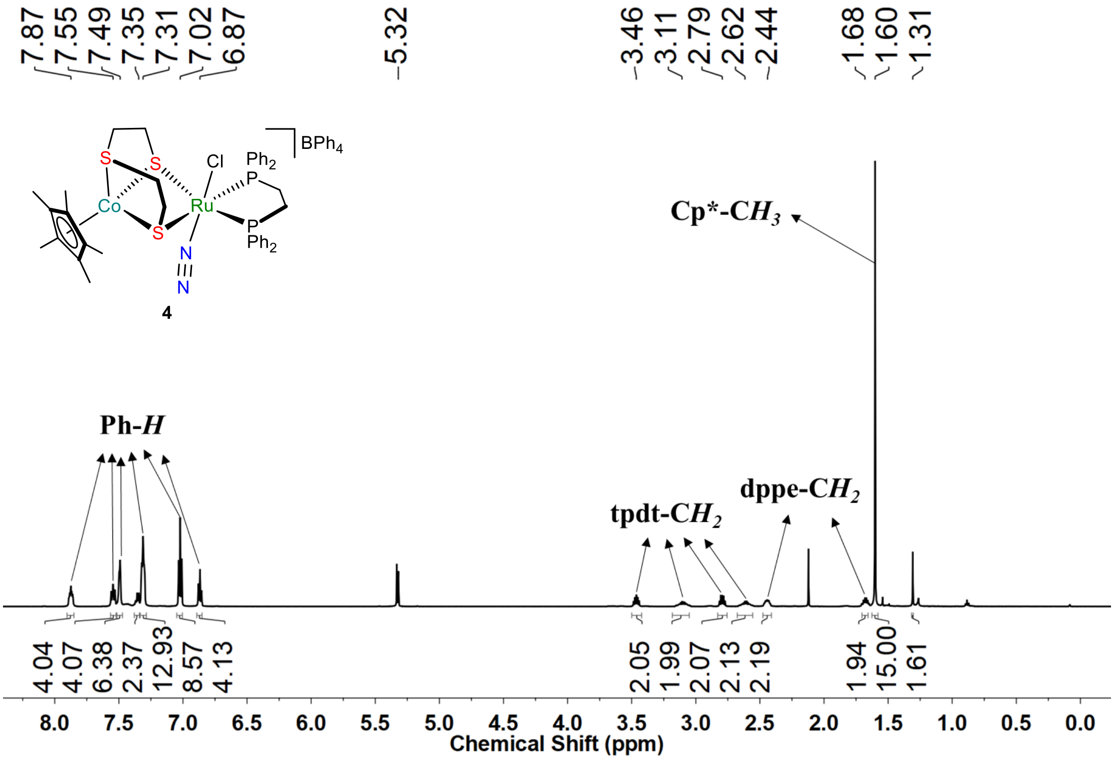

Figure S13. The $^{31}P\{^{1}H\}$ NMR spectrum of **4** in CD_2Cl_2.

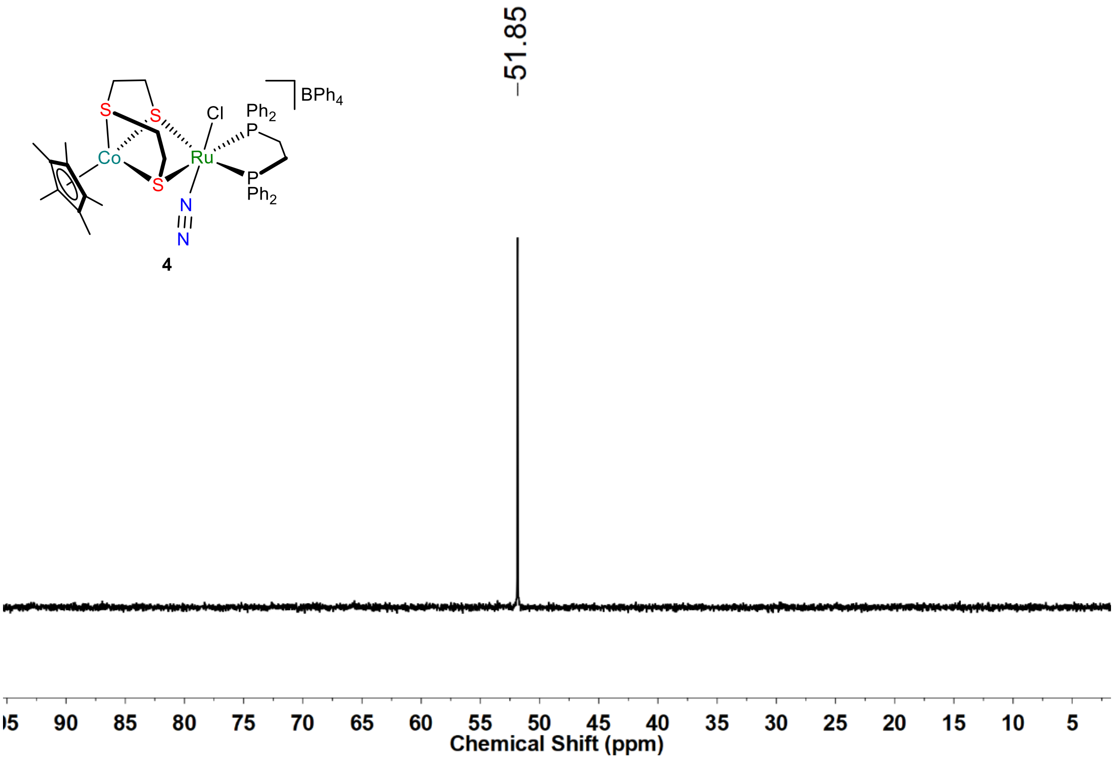

Figure S14. The ^{15}N NMR spectrum of ^{15}N-**4** in CD_2Cl_2.

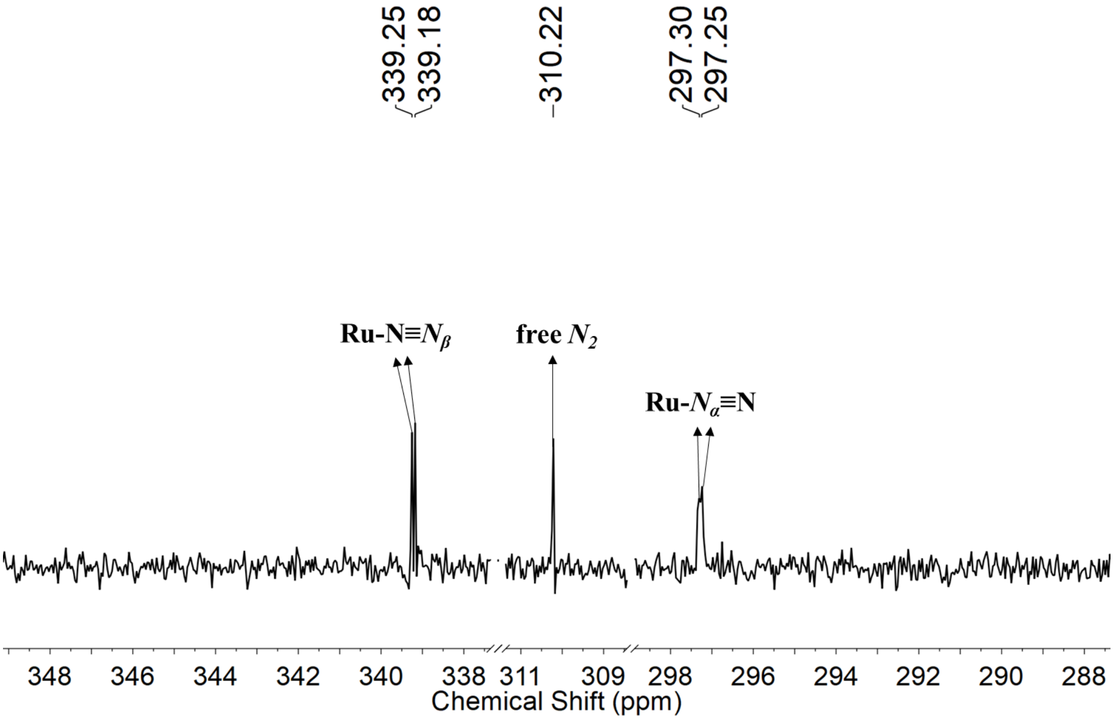

Figure S15. The ^{1}H NMR spectrum of **5** in CD_2Cl_2.

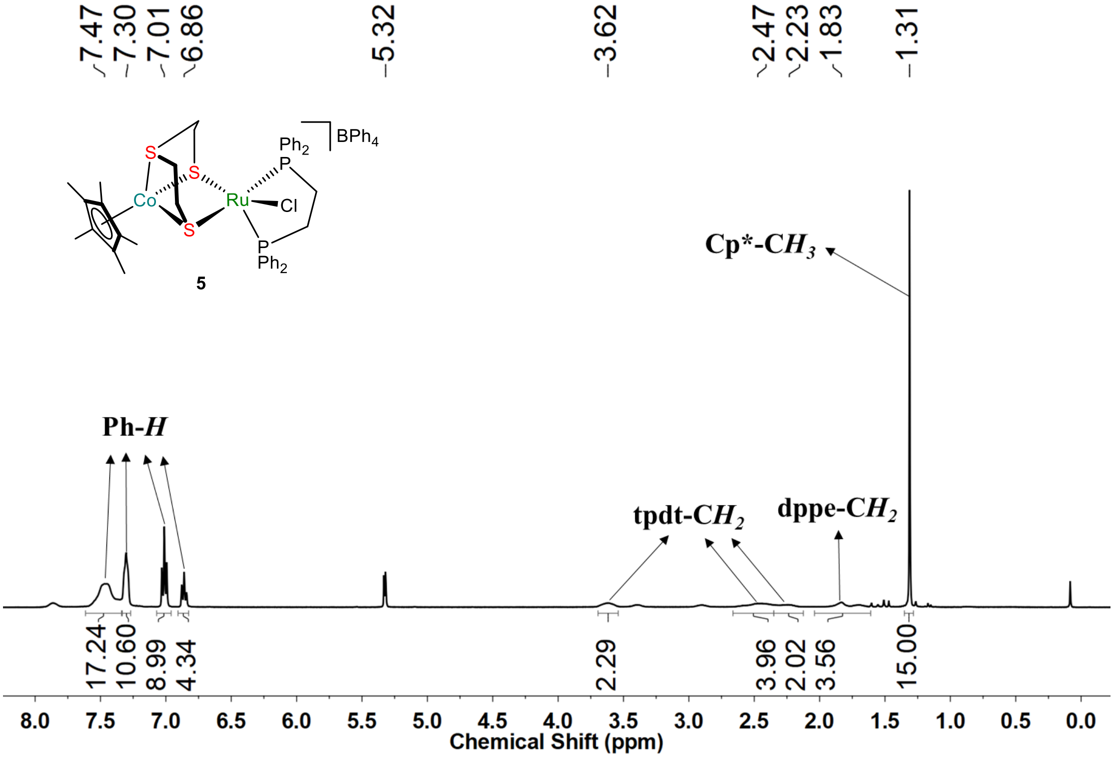

Figure S16. The $^{31}P\{^1H\}$ NMR spectrum of **5** in CD_2Cl_2.

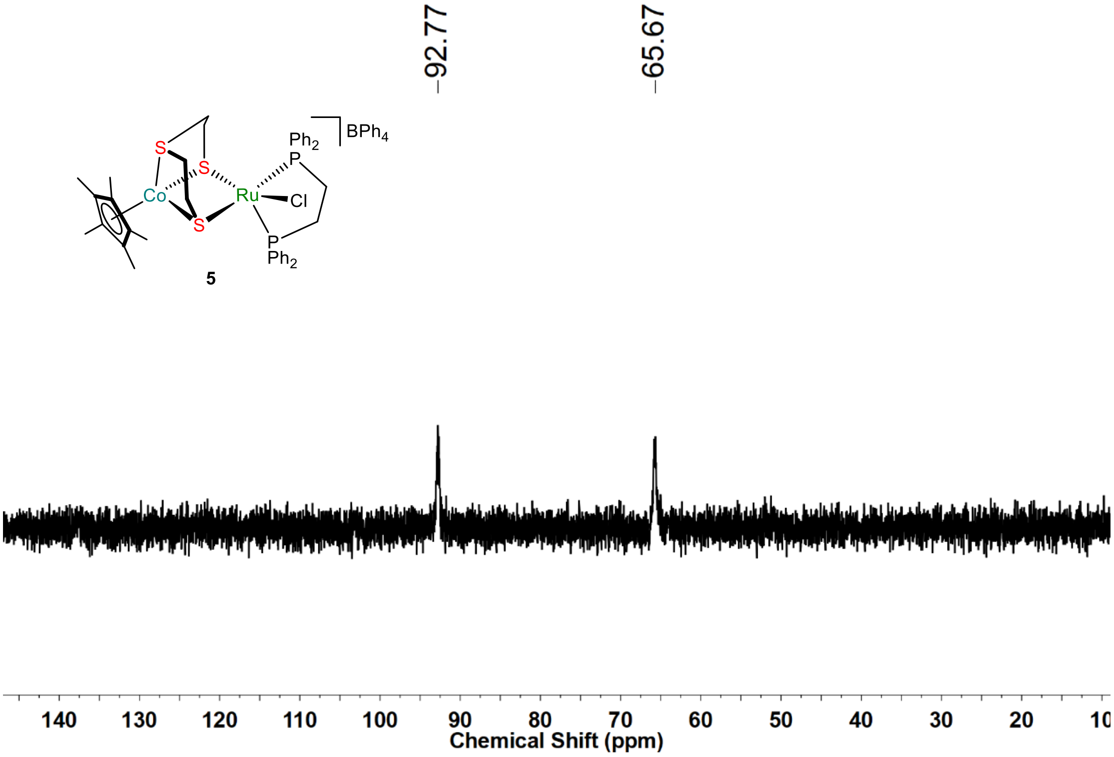

Figure S17. The time-dependent ^1H NMR spectra of the reversible conversion between **4** and **5** at 35 °C in the first 2 h and at −35 °C in the following 4 h.

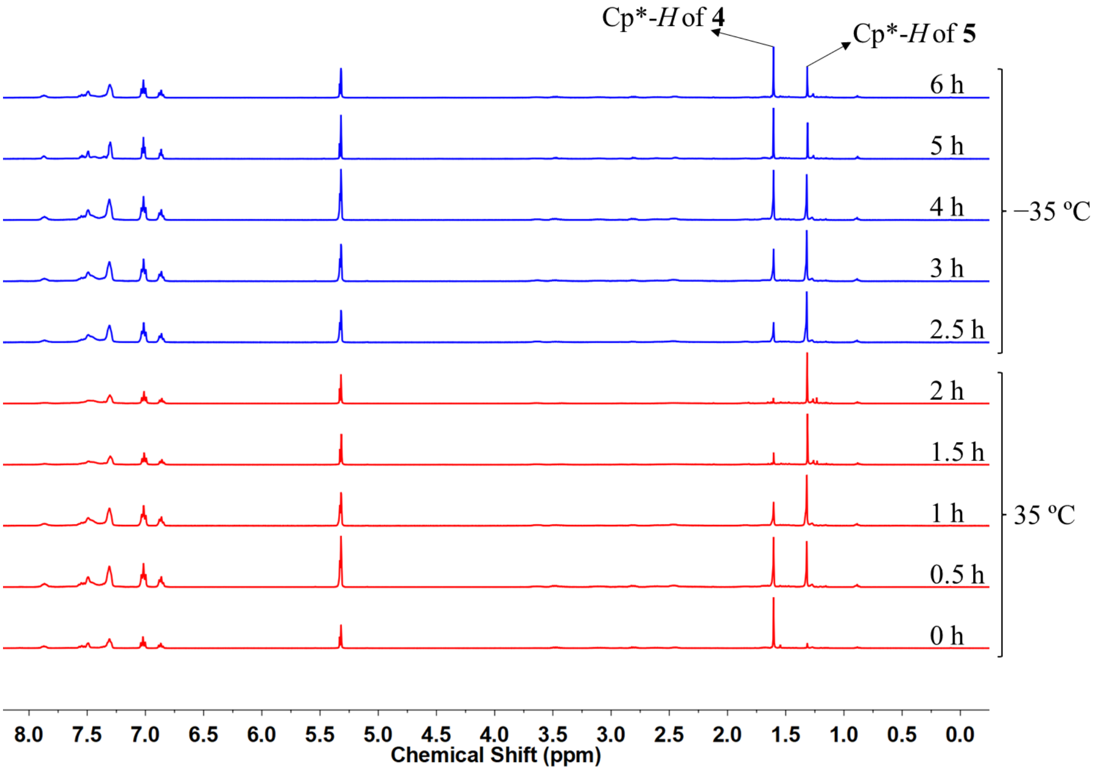

VI. IR Spectra

Figure S18. The IR (KBr) spectrum of **1**.

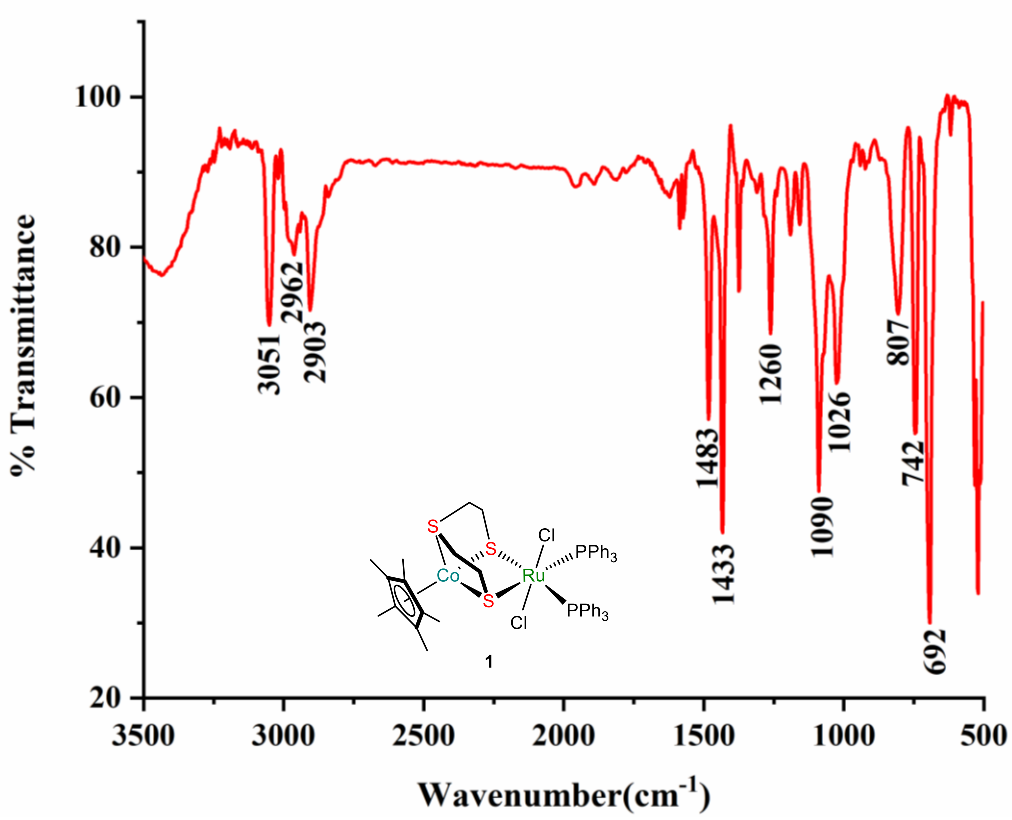

Figure S19. The IR (KBr) spectrum of **2**.

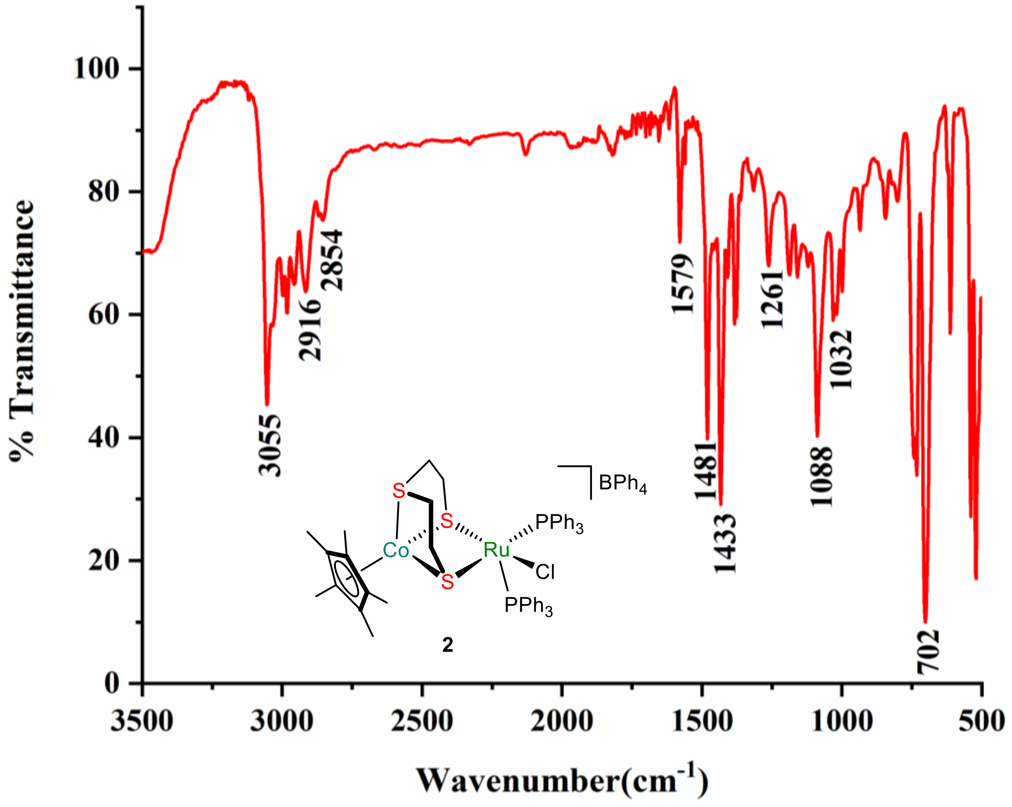

Figure S20. The IR (KBr) spectrum of **3**.

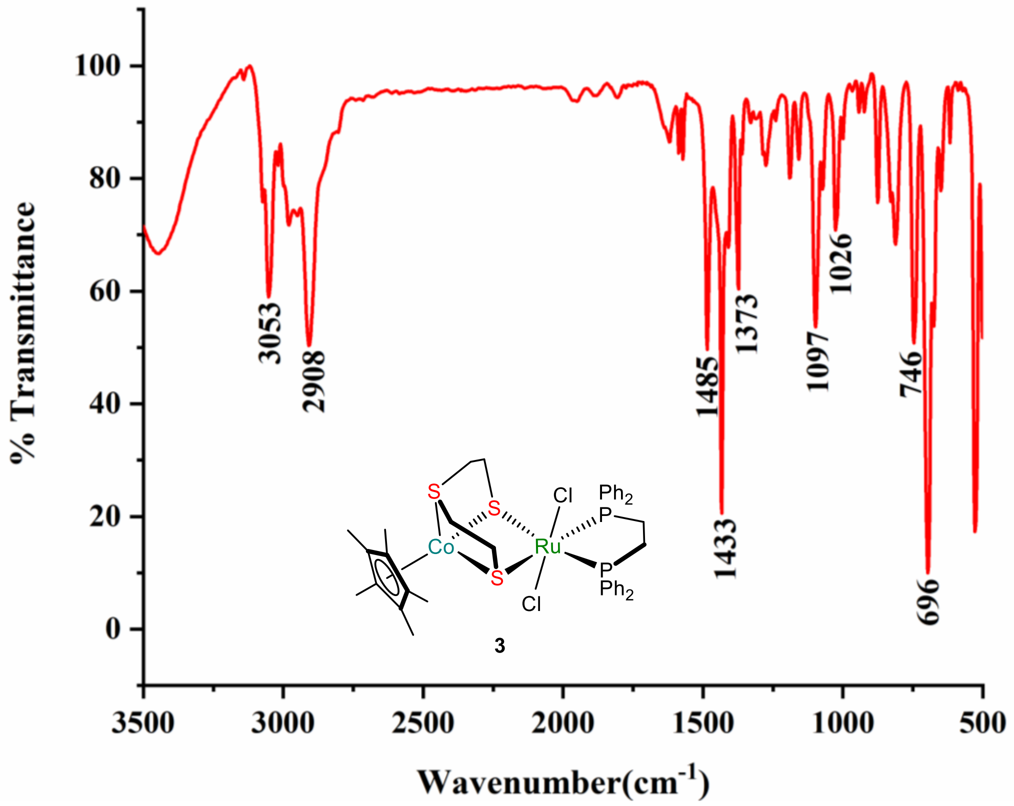

Figure S21. The IR (KBr) spectrum of **4**.

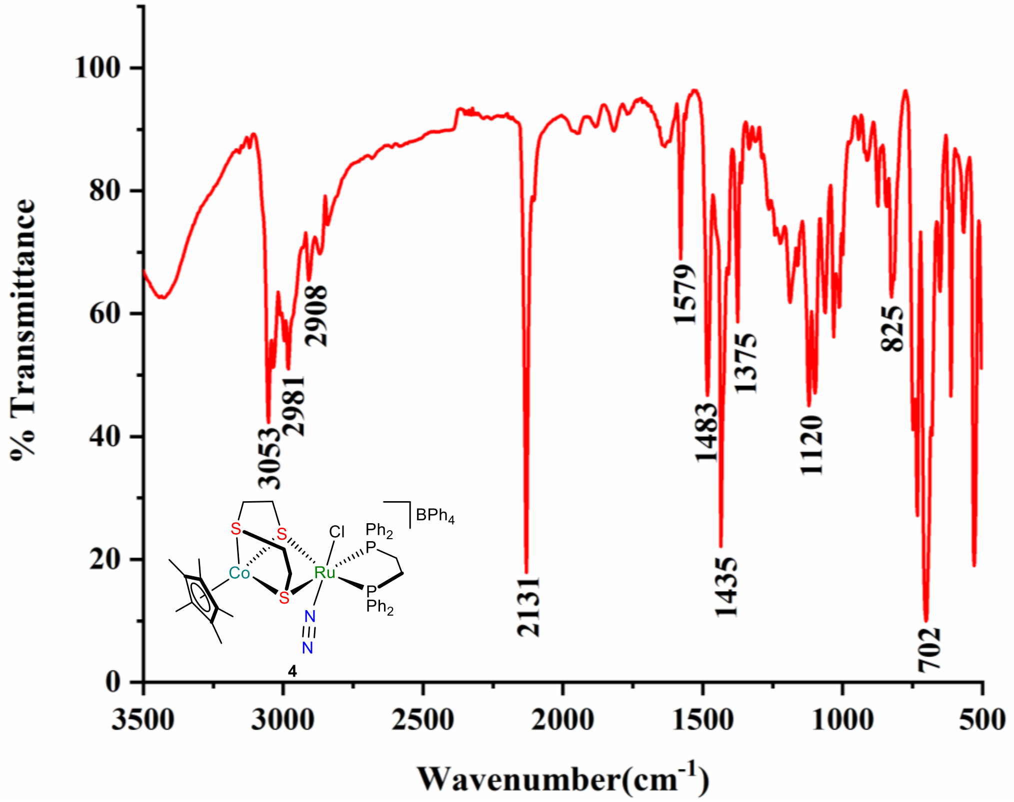

Figure S22. The IR (KBr) spectrum of ^{15}N-**4**.

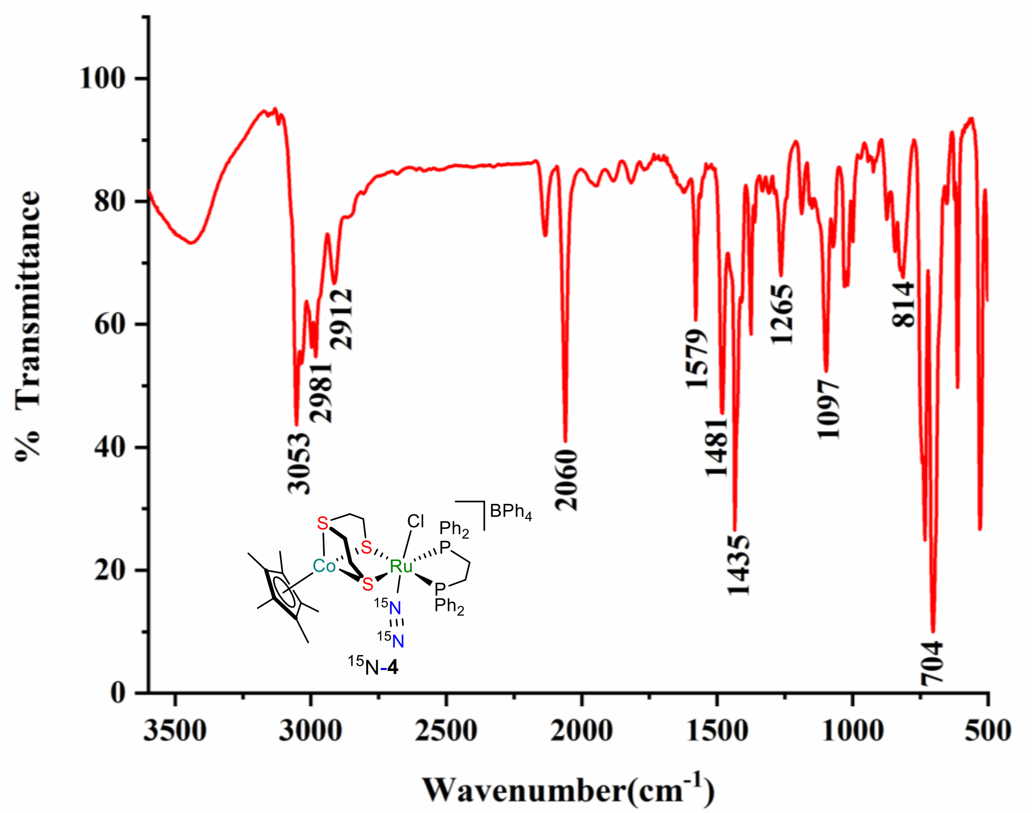

Figure S23. The overlapping IR (KBr) spectra of ^{14}N-**4** (blue) and ^{15}N-**4** (red).

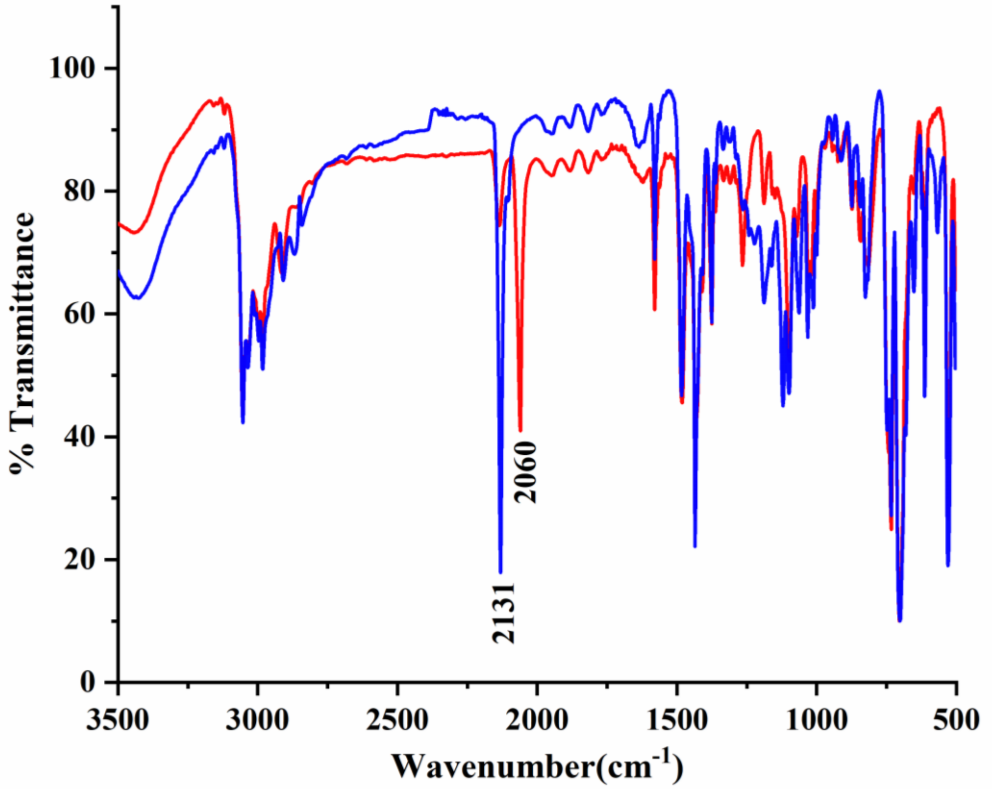

Figure S24. The IR (KBr) spectrum of **5**.

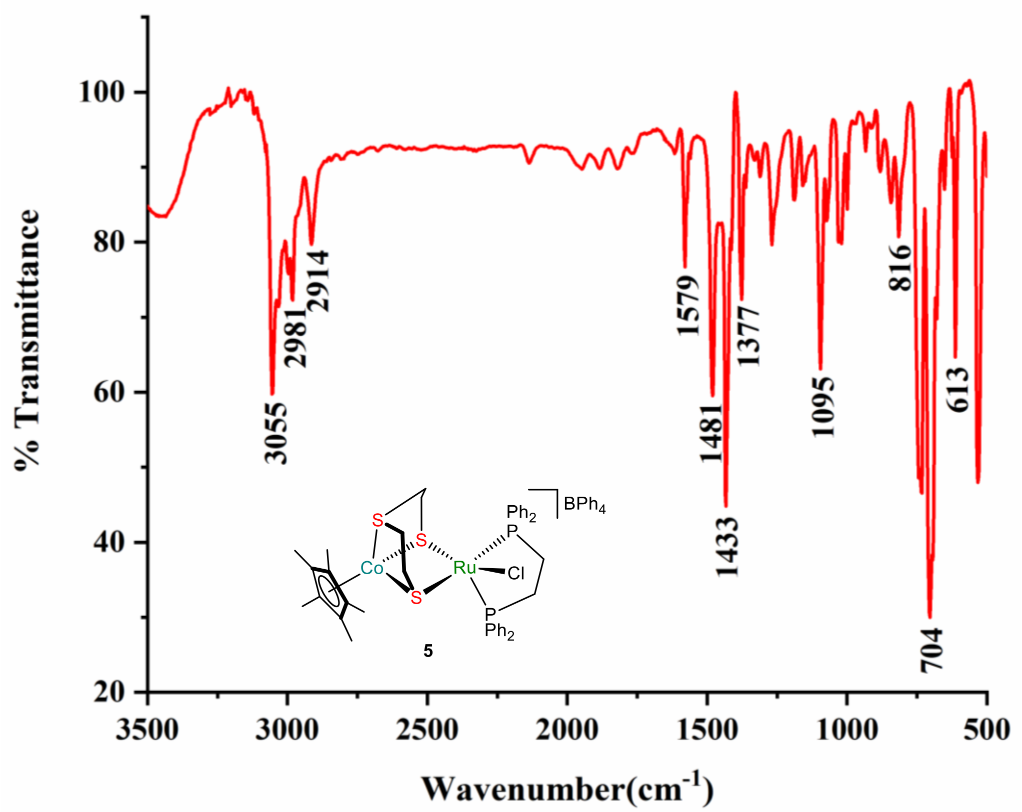

VII. ESI High Resolution Mass Spectra

Figure S25. The high resolution mass spectrum of **2** in CH_2Cl_2.

(a) The signal at *m/z* 1007.0864 corresponds to [**2**−BPh_4]$^+$. (b) Calculated isotopic distribution (upper) and the amplifying experimental diagram for [**2**−BPh_4]$^+$ (bottom).

(a)

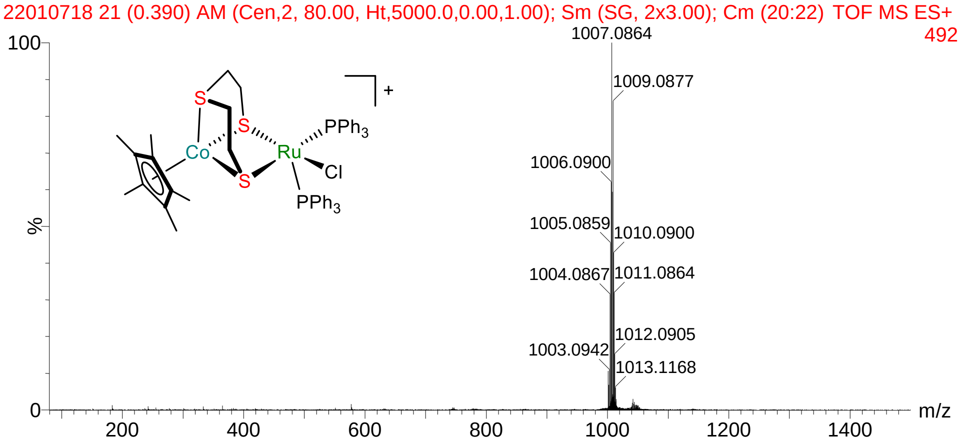

(b)

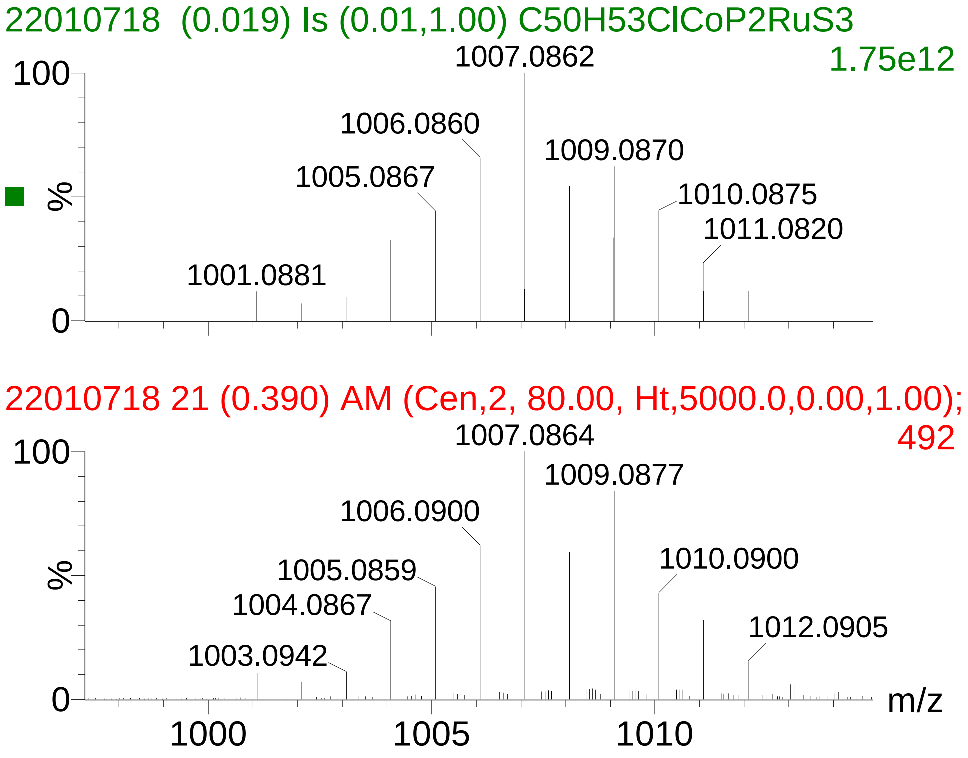

Figure S26. The high resolution mass spectrum of **4** in CH_2Cl_2.

(a) The signal at *m/z* 909.0452 corresponds to [**4**−BPh_4]$^+$. (b) Calculated isotopic distribution (upper) and the amplifying experimental diagram for [**4**−BPh_4]$^+$ (bottom).

(a)

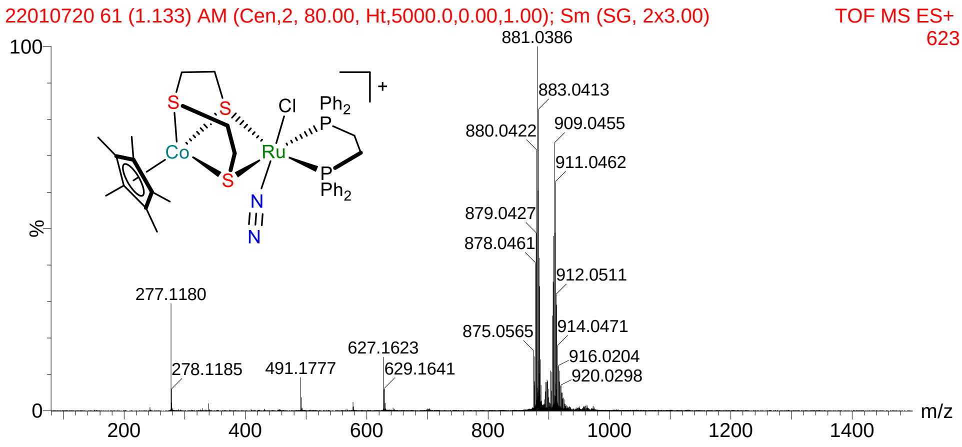

(b)

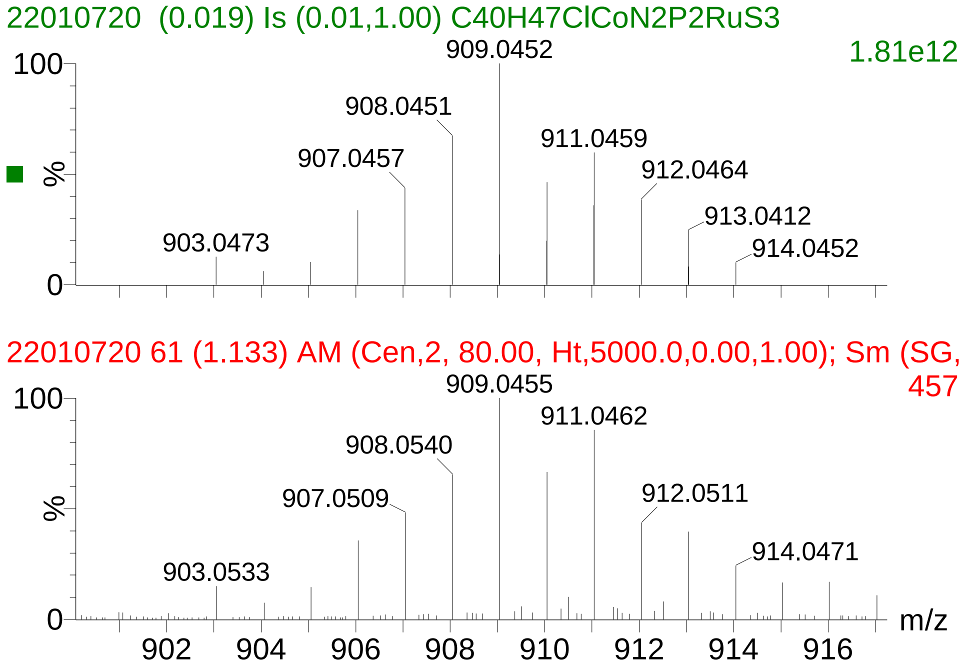

Figure S27. The high resolution mass spectrum of **5** in CH_2Cl_2.

(a) The signal at *m/z* 881.0370 corresponds to [**5**−BPh_4]$^+$. (b) Calculated isotopic distribution (upper) and the amplifying experimental diagram for [**5**−BPh_4]$^+$ (bottom).

(a)

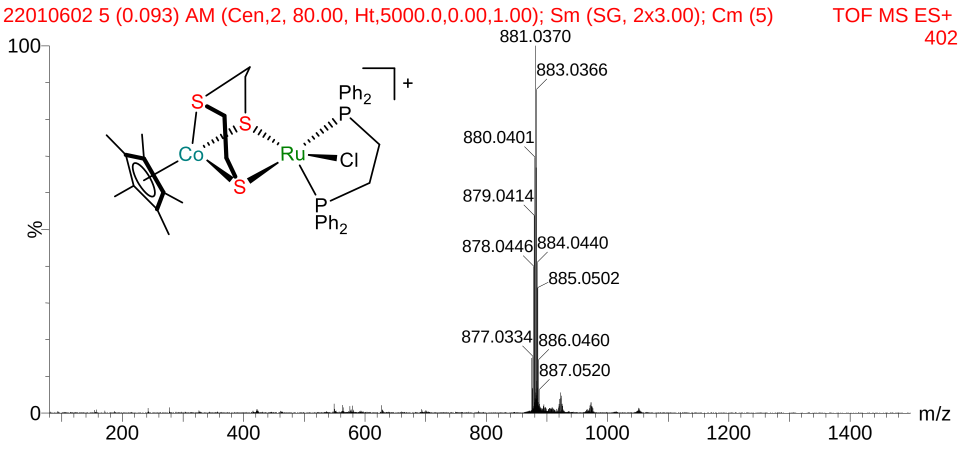

(b)

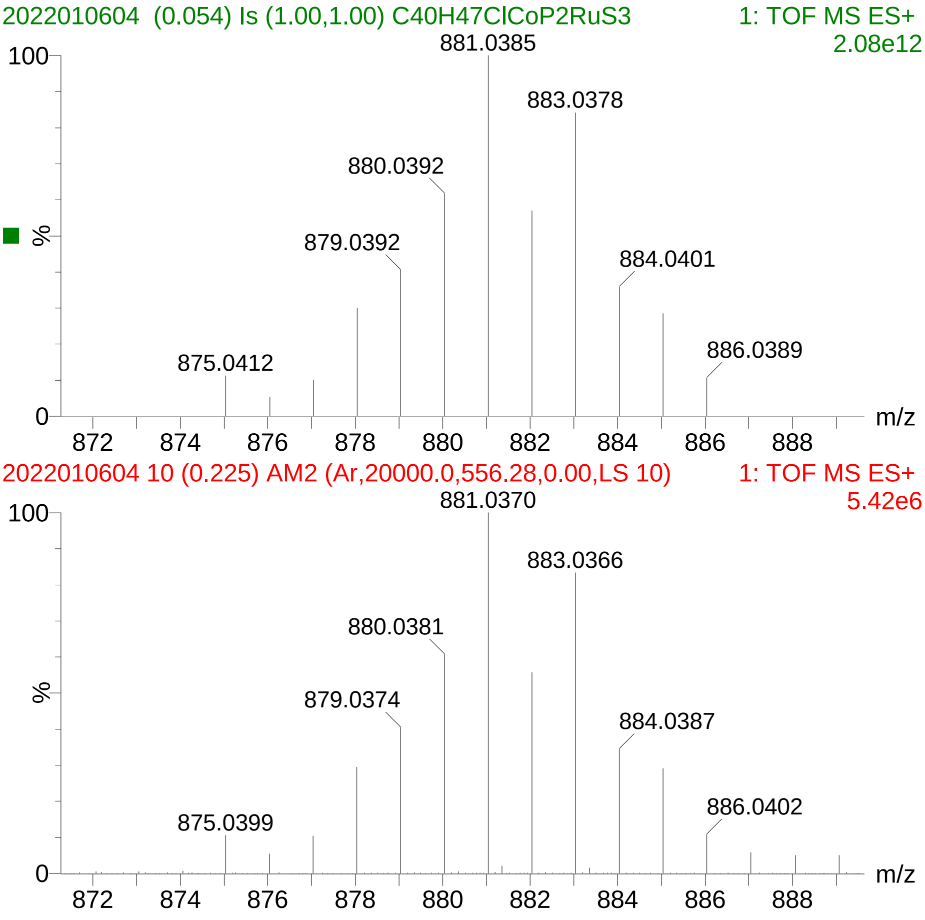

VIII. GC analysis

Figure S28. Standard working curve for quantitative GC analysis of $N(SiMe_3)_3$.

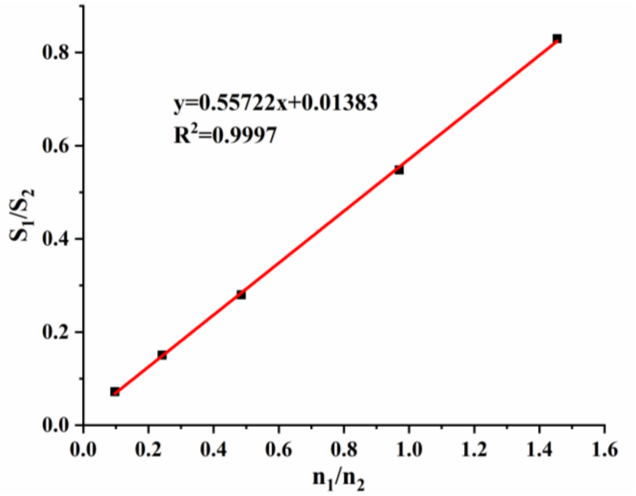

Figure S29. Typical example of GC analyses for the product mixture of the catalytic silylation reaction in **Entry 5** of **Table 1** with dodecane (20 μL) added as an internal standard.